A NEW DAMAGE FACTOR FOR SEISMIC ASSESSMENT OF DEFICIENT BARE AND FRP-RETROFITTED RC STRUCTURES

George Markou[*1,3],
Reyes Garcia[2a],
Christos Mourlas[4b],
Maurizio Guadagnini[3c],
Kypros Pilakoutas[3d],
Manolis Papadrakakis[4e]

[1]Department of Civil Engineering, University of Pretoria, South Africa
[2]School of Engineering, The University of Warwick, UK
[3]Department of Civil and Structural Engineering, The University of Sheffield, UK
[4]Department of Civil Engineering, National Technical University of Athens, Greece

Highlights

- A new 3D concrete material strategy when concrete is considered to be crushed.
- Damage factor to account cracking and rebar slippage under cyclic loading conditions.
- Validation by using experimental data on bare and FRP-retrofitted RC specimens.
- Capturing accumulated damage in concrete and steel according to the opening and closing of crack.
- 3D modeling is capturing extreme pinching on bare and FRP-retrofitted RC specimens.

ABSTRACT

The seismic assessment of reinforced concrete (RC) structures before and after retrofitting is a challenging task, mainly because existing numerical tools cannot model accurately the evolution of concrete damage. This article proposes an innovative numerical method suitable to model and assess the ultimate carrying capacity of RC structures. The modelling approach proposes a steel constitutive material model with a damage factor that accounts for accumulated damage within the surrounding concrete domain, which effectively captures bar slippage. The proposed method is validated with experimental results from full-scale cyclic tests on deficient bare and CFRP-retrofitted RC joints tested previously by the authors. The results indicate that the proposed simulation method captures the extreme nonlinearities observed in the tested RC joints, with acceptable accuracy and computational robustness. The results of this study are expected to contribute towards the development of more reliable numerical tools and design guidelines for efficient seismic assessment of RC structures before and after earthquakes.

Keywords: Beam-column RC joints; Finite Element Modelling; FRP strengthening; Bar Slippage; Cyclic Nonlinear Analysis.

1. Introduction

Many seismically active countries have large numbers of reinforced concrete (RC) structures that were designed either using old design codes or without accounting for seismic loads. Post-earthquake missions have revealed that critical elements of such structures (e.g. columns and beam-column joints)

[*]Corresponding Author, Associate Professor, E-mail: george.markou@up.ac.za, g.markou@sheffield.ac.uk
[a]Assistant Professor: reyes.garcia@warwick.ac.uk
[b]Ph.D., E-mail: mourlasch@central.ntua.gr
[c]Senior Lecturer: m.guadagnini@sheffield.ac.uk
[d]Professor, E-mail: k.pilakoutas@sheffield.ac.uk
[e]Professor, E-mail: mpapadra@central.ntua.gr

had insufficient shear reinforcement and inadequate bar anchorage lengths, which led to structural collapses and consequently to huge human and financial losses [1]. To minimise damage and human/financial losses during earthquakes, engineers utilise assessment and retrofitting techniques that, nowadays, are incorporated into modern seismic codes.

Over the last decades, engineers have also developed some practical numerical and computational tools to seismically assess existing RC structures. However, such assessments before and after retrofitting are challenging, mainly because a) the progression of concrete damage and b) the effect of the retrofitting intervention are difficult to capture by existing models and simulation software. To address these drawbacks, the authors have recently proposed a new Hybrid Modelling (HYMOD) approach that provides numerically objective, accurate and computationally robust solutions to the assessment of the ultimate carrying capacity of retrofitted structures [2]. The approach proved effective in modelling the seismic behaviour of a 4-storey RC building [3] subjected to pseudo-dynamic tests in bare and retrofitted conditions for which experimental data were available. The building was strengthened with infill RC shear walls and Carbon Fibre Reinforced Polymer (CFRP) jackets at its base. For the discretization of the shear-dominated concrete domain 8-noded hexahedral finite elements were used, whereas the reinforcement was modelled with embedded beam elements. The numerical results presented in [3] captured accurately the experimentally-derived base shear. However, pinching effects were not well captured because concrete material deterioration and potential bar slippage at the building base were not incorporated into the adopted constitutive material models of steel and concrete.

Previous studies have proposed several models/approaches that try to capture extreme nonlinear RC structural behaviour under cyclic conditions. Lykidis and Spiliopoulos [4] proposed a 3D detailed modelling approach that uses 20-noded hexahedral finite elements and simulated cracking with the smeared crack method, and discretised reinforcement with embedded rod elements. The model in [4] included an additional degree of freedom (dof) per embedded bar to account for bar slippage. Although Lykidis and Spiliopoulos' model captured accurately the experimental results of a corner beam-column RC joint that exhibited slippage and concrete damage, the model did not capture pinching when used to simulate the behaviour of internal RC joints. This can be attributed to the inability of the concrete and steel material models to capture accumulated damage due to crack opening and closing during cyclic loading, and to the effect of bar slippage on the overall behaviour of the joints.

Previous studies have also proposed a number of numerical modelling approaches to simulate the behaviour of retrofitted RC and masonry structures under monotonic loading [5-31]. However, none of these proposed models can capture cyclic behaviour unless calibrated moment rotation elements are used. For example, Cortés-Puentes and Palermo [32] investigated the cyclic behavior of RC shear walls strengthened with different CFRP configurations. The numerical analyses were carried out using the 2D finite element software VecTor2. Whilst the numerical results predicted well the experimental load-deformation loops, the modelling approach is only applicable to 2D problems.

Mourlas et al. 2019 [33] extended the work in [34, 35] to carry out 3D nonlinear cyclic analysis and proposed the use of two material damage factors so as to take into account the effect of opening and closing of cracks within a concrete hexahedral finite element that captures cracking using the smeared crack approach. The results in [33] confirmed that the proposed integration of the concrete and steel material models with the respective damage factors predicted very well the static and dynamic nonlinear behaviour of concrete structures with pinching. The modelling method proposed in [33] captured the cyclic behaviour of RC structures with pinching without the need of introducing additional degrees of fredom that would have made computations more intensive.

In this work, the material model of steel, as presented in [33], was integrated with a new reduction factor, which is defined by the accumulated damage of crack opening/closing, in order to reduce the stiffness of the steel reinforcement in the cracked concrete region within which slippage is expected to occur. This article investigates the ability of the proposed material model to capture the overall mechanical response of severely damaged concrete joints characterized by intense pinching phenomena. The proposed modelling method is validated with results of bare and retrofitted RC joints tested previously by the authors. Section 3 presents a brief description of the experimental programme reported in [36]. Both phases are modelled and analysed in Section 4. Conclusions and future work

will be given in Section 5.

2. Material Modelling

This section introduces the concrete and steel material models, as well as the new damage factors. The proposed material model is based on the triaxial behaviour of concrete taking into account the effect of opening and closing of cracks, in capturing strength and stiffness degradation, and pinching effects.

2.1 Concrete Material Modelling and Damage Factor

The constitutive modelling of concrete, which is an extension of the research work presented by Kotsovos and Pavlovic [4] as it is described in [34], has the following constitutive relations:

$$\varepsilon_0 = \varepsilon_{0(h)} + \varepsilon_{0(d)} = (\sigma_0 + \sigma_{id}) / (3K_s) \tag{1}$$

$$\gamma_0 = \gamma_{0(d)} = \tau_0 / (2G_s) \tag{2}$$

The parameters K_s and G_s of Eqs 1 and 2 are the secant bulk and shear moduli, respectively. For more information on the concrete material model one may refer to [4, 34]. According to the adopted model for the needs of this research work, the model adopts a smeared crack approach (see Fig. 1) by simulating the geometrical discontinuity through the assumption of a displacement continuity. During the nonlinear solution procedure, it is assumed that the crack opening can occur at any Gauss Point without any constraints [9], therefore, the crack formation or closure state is treated in a unified way within every internal iteration. When a crack opens, the material properties normal to the crack plane are set to zero and the concrete material model assumes the total loss all of its carrying capacity perpendicular to the crack. The strength envelope of concrete is given in Eq. 3 and it is based on the William and Warkne [37] formulae.

$$\tau_{0u} = \frac{2\tau_{0c}(\tau_{0c}^2 - \tau_{0e}^2)\cos\theta + \tau_{0c}(2\tau_{0e} - \tau_{0c})\sqrt{4(\tau_{0c}^2 - \tau_{0e}^2)\cos^2\theta + 5\tau_{0e}^2 - 4\tau_{0c}^2\tau_{0e}^2}}{4(\tau_{0c}^2 - \tau_{0e}^2)\cos^2\theta + (2\tau_{0e} - \tau_{0c})^2} \tag{3}$$

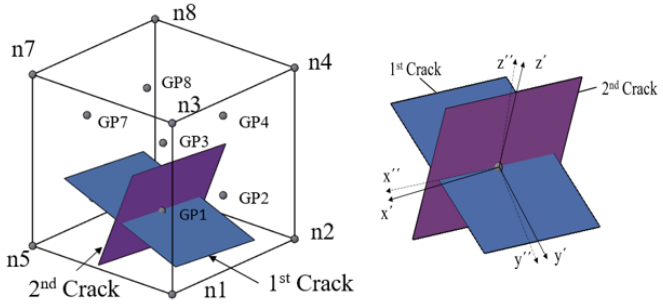

Figure 1: Two cracks open at a single Gauss Point. Local axes. [33].

Additionally, the crack closing criterion that was proposed by Mourlas et al. [33] in adopted for the needs of this research work. This numerical criterion was critical in achieving a faster convergence ratio during the cyclic load analysis. Accordingly, the closure of cracks is expressed as:

$$\varepsilon_i \le \left(b - \frac{n_{cr} - 1}{n_{tot}} \right) \cdot \varepsilon_{cr} \tag{4}$$

where ε_i represents the current strain along the i-direction which is normal to the plane of the crack; ε_{cr} is the strain for which the cracking formation occurs; b equals to the number of the imposed displacement branches of the load history; n_{cr} is the increment that the crack formed at; and n_{tot} is equal to the increments that a single displacement branch was divided into.

During the nonlinear analysis, if the criterion of crack-closure is found to be satisfied at a specific Gauss Point that had only one prior crack formation, then part of the stiffness is assumed to be lost along the previous crack plane (material deterioration) that formed perpendicular to the maximum

principle tensile stress. Based on the above, the constitutive matrix is expressed as follows:

$$\boldsymbol{C}_l = \begin{bmatrix} a_n\cdot(1-D_c)\cdot(2G_t+\mu) & a_n\cdot(1-D_c)\cdot\mu & a_n\cdot(1-D_c)\cdot\mu & 0 & 0 & 0 \\ a_n\cdot(1-D_c)\cdot\mu & a_n\cdot(1-D_c)\cdot(2G_t+\mu) & a_n\cdot(1-D_c)\cdot\mu & 0 & 0 & 0 \\ a_n\cdot(1-D_c)\cdot\mu & a_n\cdot(1-D_c)\cdot\mu & 2G_t+\mu & 0 & 0 & 0 \\ 0 & 0 & 0 & a_s\cdot(1-D_c)\cdot\beta\cdot G_t & 0 & 0 \\ 0 & 0 & 0 & 0 & a_s\cdot(1-D_c)\cdot\beta\cdot G_t & 0 \\ 0 & 0 & 0 & 0 & 0 & a_s\cdot(1-D_c)\cdot\beta\cdot G_t \end{bmatrix} \quad (5)$$

where β is a shear strength retention factor. Based on the parametric investigation presented in [33], constants a_n and a_s are assumed to have values of 0.25 and 0.125, respectively.

The proposed expression in Eq. 5 that describes the anisotropic behaviour of concrete at the local Cartesian coordinate system must be transformed into the global system through the use of basic transformation laws:

$$\boldsymbol{C}_g = \boldsymbol{T}^T \boldsymbol{C}_l \boldsymbol{T} \quad (6)$$

where $\boldsymbol{T}$ is the corresponding transformation matrix consisted by the direction cosines that define the orientation of the local to global axis; D_c is a damage factor proposed in [33] that describes the accumulated loss of energy based on the current number of times a crack was found to opened and closed during the nonlinear solution procedure. D_c is calculated as follows [33]:

$$D_c = e^{-(1-a)/f_{cc}} = e^{-\left(1-\left(1-\frac{\varepsilon_{cr}}{\varepsilon_{\max}}\right)\right)/f_{cc}} = e^{-\left(\frac{\varepsilon_{cr}}{\varepsilon_{\max}}\right)/f_{cc}} \quad (7)$$

where f_{cc} represents how many times a crack has closed and it is updated in every iteration at each Gauss Point. Fig. 2 shows the variation of D_c (Eq. 7) as a function of parameter a and for different values of f_{cc}.

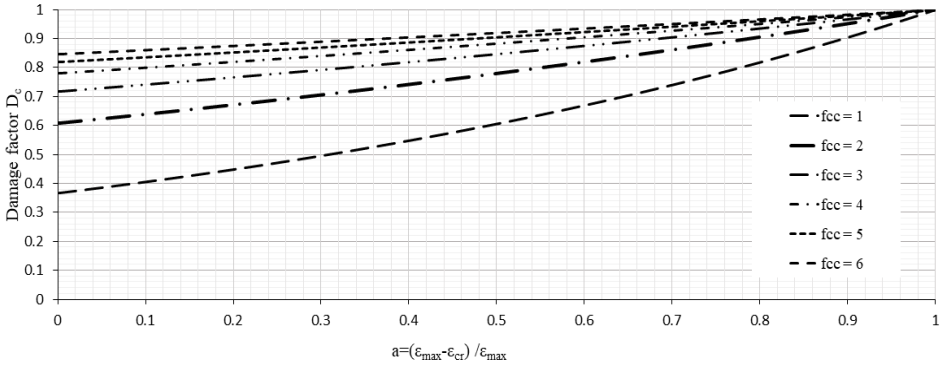

Figure 2: Damage factor D_c (Eq. 7) vs parameter a for different f_{cc} values [33].

During nonlinear analysis, the constitutive matrix is calculated from Eq. 5, for the case where a crack is being closed at a Gauss Point and had previously one or two cracks already opened from previous increments. After a crack closure is completed, the stresses are then corrected through the use of Eq. 8.

$$\boldsymbol{\sigma}^j = \boldsymbol{\sigma}^{j-1} + \boldsymbol{C}_g \cdot \Delta\boldsymbol{\varepsilon}^j \quad (8)$$

Finally, once all cracks have closed (at previously cracked Gauss Points) and the reduction factor a (in Eq. 4) of one of the cracks that already closed is larger than 0.5, then the corresponding constitutive matrix is computed according to Eq. 9.

$$\boldsymbol{C}_g{}' = (1-D_c)\cdot\boldsymbol{C}_g \quad (9)$$

As an additional step and in an attempt to introduce a stabilizing factor during cyclic modelling of

extremely cracked concrete regions that were studied in this research work and presented in Section 4, the modification of the constitutive matrix of a fully crushed Gauss Point is proposed to take the following form:

$$\boldsymbol{C}_t^{'}=\begin{bmatrix} \beta_c\cdot(1-D_c)\cdot(2G_t+\mu) & 0 & 0 & 0 & 0 & 0 \\ 0 & \beta_c\cdot(1-D_c)\cdot(2G_t+\mu) & 0 & 0 & 0 & 0 \\ 0 & 0 & \beta_c\cdot(1-D_c)\cdot(2G_t+\mu) & 0 & 0 & 0 \\ 0 & 0 & 0 & \beta_c\cdot(1-D_c)\cdot\beta\cdot G_t & 0 & 0 \\ 0 & 0 & 0 & 0 & \beta_c\cdot(1-D_c)\cdot\beta\cdot G_t & 0 \\ 0 & 0 & 0 & 0 & 0 & \beta_c\cdot(1-D_c)\cdot\beta\cdot G_t \end{bmatrix} \quad (10)$$

where $\beta_c = 0.025$ which is a parameter similar to β that represents the shear strength retention factor; D_c represents the damage factor from Eq. 7. When a Gauss Point is crushed, the material model foresees that the point has lost its resistance, but due to the proposed constitutive matrix of Eq. 10, the Gauss Point has the ability to maintain a resistance which decreases as the compressive cracks increase. Thus, a crushed Gauss Point's cracks will remain open, but do maintain a low residual stiffness, which was found to introduce numerical stability when excessive cracking occurs. This remaining stiffness resistance is necessary when dealing with modelling RC structures subjected to high compressive loads or joints that develop excessive diagonal cracks or intense concrete spalling.

2.2 Steel Material Modelling and New Damage Factor

The damage level that will occur because of the opening of cracks at a specific region also affects the bond state between steel rebar and the concrete surrounding it (slippage will eventually occur). Consequently, this damage mechanism directly affects the force transfer between the steel reinforcement to the surrounding concrete domain, especially in the anchorage areas. Therefore, the modification of the stress-strain relationship for steel, published by Menegotto-Pinto [37], is proposed here to account for the degree of concrete damage surrounding the rebar element during the nonlinear cyclic analysis. The loss of bond between bars and surrounding cracked concrete is accounted for indirectly by reducing the stiffness contribution of the bars [33], which in turn is expected to contribute to the pinching effects. Thus, the use of a bond-slip model that would require defining new material parameters and an additional dof at each bar, is avoided.

Based on the proposed formulation presented in [33], the average of all reduction parameters *a,* expressed by Eq. 12, at the 8 Gauss Points of any concrete hexahedral element, can be used to determine the damage level D_s of concrete by using Eq. 11.

$$D_s = \left[1 - a_{Element}\right] \quad (11)$$

$$a_{Element} = \frac{\sum_{1}^{n_{cr}} a_i}{n_{cr}}, \quad (12)$$

where n_{cr} is the total number of current cracked Gauss Points.

During unloading and when the structure reaches its initial deformation, the material deterioration of the rebars can be calculated as:

$$E_s^{'} = (1 - D_s)E_s \quad (13)$$

The material deterioration is activated when the criterion $\sigma_s \cdot \varepsilon_s < 0$ is satisfied, which represents the state when crack closing and re-opening occur, where the pinching phenomena are significant. In addition to the proposed modification in [33] and in order to capture pinching effects at the material level, the implementation of a reduced parameter *R* of the steel model [38] is proposed here:

$$R = R_0 - \frac{a_1 \xi}{\alpha_2 + \xi} \tag{14}$$

The values of R_0, a_1 and a_2 were determined by extensive numerical tests performed in [33] and are assumed to be 20, 18.5 and 0.15, respectively. By using the same concept described above and as presented in [33], the reduction factor D_R is proposed herein in order to decrease the parameter R into R' which is calculated as:

$$R' = (1 - D_R) R \text{ , where } D_R = D_s \tag{15}$$

Fig. 3 shows the σ-ε curves of the modified steel material model with different steel damage factor D_S levels as proposed in [33], while Fig. 4 shows the modification of the Menegotto-Pinto material model with the new steel damage factor D_R proposed in this study for different damage levels of concrete. Fig. 4 shows that the damage factor D_R modifies the stress-strain curves of the steel model in a similar manner to the D_S damage factor for concrete. However, in the case of D_R, the hysteretic loops of the material model tend to inflict a higher energy decrease as the accumulated damage in the surrounding concrete increases. This modified Menegotto-Pinto steel material model was found through preliminary parametric studies to be capable of capturing nonlinearities in excessively cracked concrete around steel rebars manifested by rebar slip and significant energy losses within these regions.

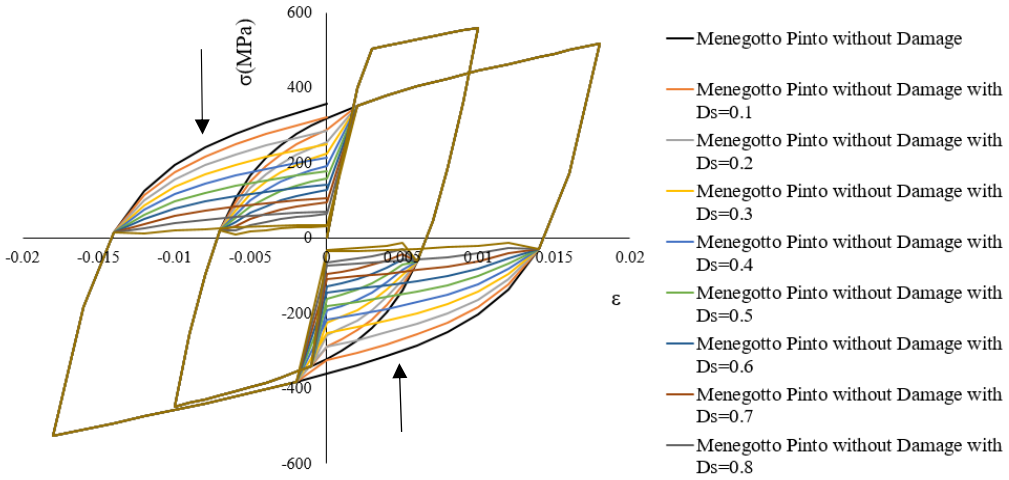

Figure 3: Modified Menegotto-Pinto steel model with parameters E′ (Eq. 13) for different damage factor (D_S) values.

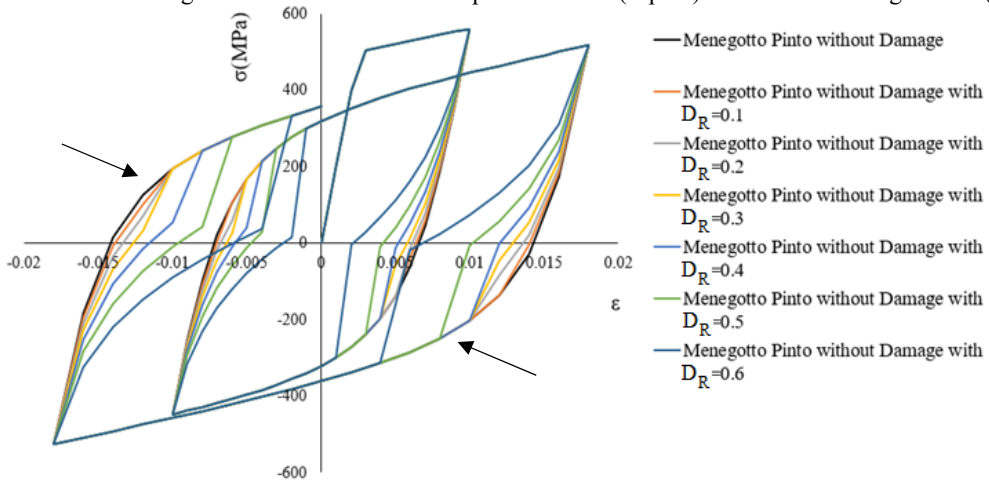

Figure 4: Modified Menegotto-Pinto steel model with parameter R′ (Eq. 15) due to the opening and closing of cracks for different damage factor (D_R) values.

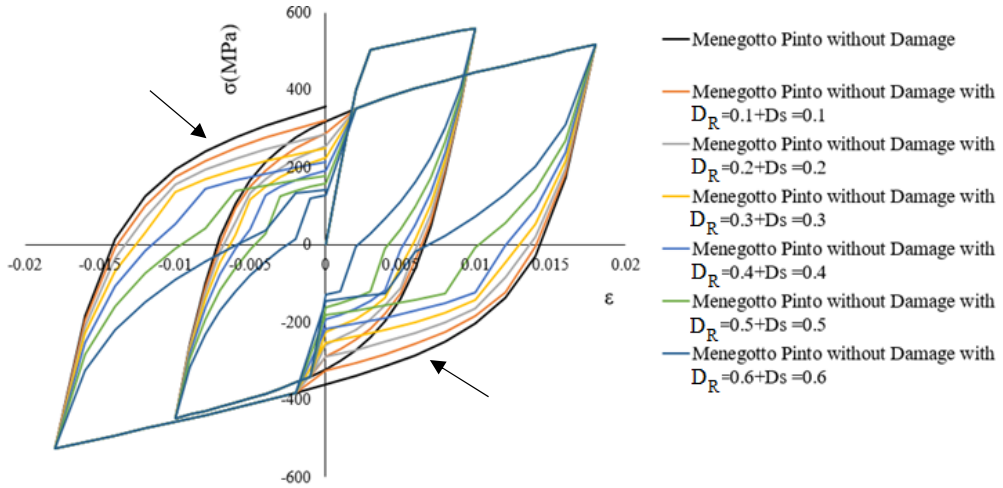

Figure 5: Modified Menegotto-Pinto steel model with parameters E′ (Eq.13) and R′ (Eq. 15) for different damage factors (D_R and D_S) values.

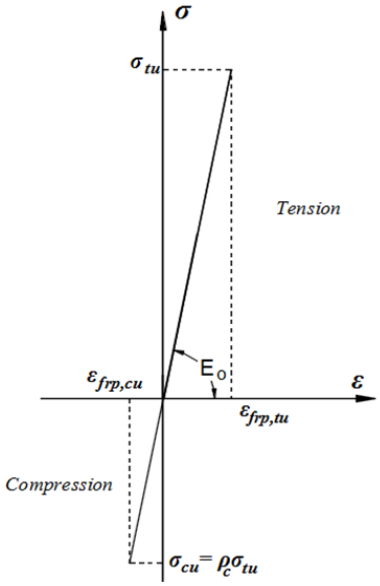

Figure 6: CFRP jacketing material model [39].

The stress-strain graph of the modified Menegotto-Pinto model with both steel damage factors *(D_S* and *D_R)* being active, can be seen in Fig. 5 for different levels of concrete damage. The modified Menegotto-Pinto material model of Fig. 5, accounts for bar slip and other nonlinear phenomena that occur within the excessively cracked concrete regions. This is expected to capture different damage levels based on the cracks that occur at each Gauss Point within the concrete hexahedral elements. Indeed, the new damage factor *D_R* affects the hysteretic loops so that the higher the damage is within the concrete domain, the more the steel mechanical response is affected through a decrease in energy absorption, thus leading to smaller hysteretic loops. This also affects the corresponding internal force transferred from the bar to the concrete domain, simulating in this way the mechanism that occurs when slip initiates within a heavily cracked concrete region due to the loss of bond.

The σ-ε relationship of the CFRP jacketing is assumed to be linear until failure occurs in both tension and compression (Fig. 6). As it can be seen, loss of capacity was assumed to occur when the ultimate stress at any Gauss Point of the CFRP hexahedral elements was reached. According to the reported material properties [36], the ultimate CFRP tensile strength was 4,140 MPa and the elastic modulus was 241 GPa. It was also assumed that the CFRP hexahedral elements used to discretize the jacketing were fully bonded to the concrete finite elements.

3. Experimental Data

The proposed modelling approach presented in section 2 is validated using experimental results from three full-scale cyclic tests on deficient bare and CFRP-retrofitted RC joints tested previously by the authors [36]. The specimens were used to investigate a 2D exterior as a part of a multi-storey moment-resisting frame, where the slabs were excluded for the needs of this experiment [36] (see **Figure 7**a). **Figure 7**b shows the cross sections and longitudinal reinforcement of column and beam. The longitudinal column bars were lapped for a length 400 mm just above the joint core to represent typical deficient construction practices. Two types of anchorage detailing (types A and B) were examined, as shown in **Figure 7**c. The short straight anchorages of the beam were designed to be insufficient in order to initiate slippage of the 16 mm rebars. The column-to-beam flexural strength ratio ($\sum MR_{col}/\sum MR_{beam}$) was approximately 1.0, therefore, the joint did not satisfy the strong column-weak beam strength hierarchy. Accordingly, the specimens were intentionally designed to fail at the joint core, which was let without any confining stirrups. Furthermore, to prevent a shear failure outside the joint core 8 mm in diameter stirrups were used for both the column and beam, with a 150 mm spacing.

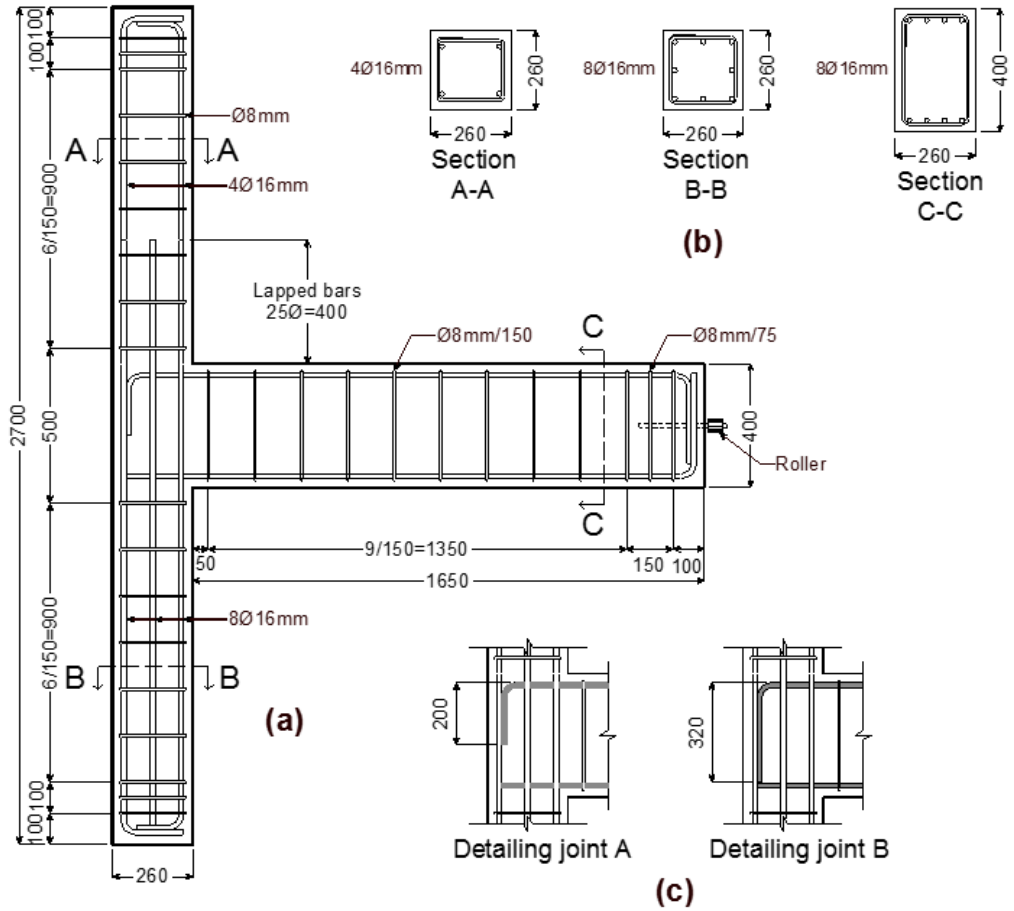

Figure 7: Reinforcement details and geometry of the RC joints (units: mm) [36].

Table 1 shows the ID code of the specimens, as well as the concrete strength (f_{cm}), tensile concrete strength (f_{ctm}) and test condition [36]. The first letter of the ID stands for "Joint", and the second for the type of detailing (A or B). Joints JA2 and JB2 were initially tested in bare condition to produce severe damage at the core, according to the test setup shown in **Figure 8**, where the column is shown laying horizontally. The cyclic load during each experimental test was directly applied to the beam using a servo-hydraulic actuator (in displacement control). Three complete cycles were applied for each assumed drift ratio δ (δ = beam tip displacement/beam length) ranging from ±0.25% and up to ±5.0%. After the initial tests on joint JB2, the core's damaged concrete was completely removed and

replaced with highly flowable concrete. Thereafter, the joint was retrofitted with externally bonded CFRP sheets, and the specimen was renamed as JB2RF. The main goal of the CFRP retrofitting intervention was to i) prevent premature failure of the core zone, and ii) enhance the flexural capacity of the column. Failure of specimen JB2RF was dominated by the rupture of the CFRP sheets at drift ratios $\delta = \pm 5.0\%$. **Figure 9** shows the final failure of specimens JB2 and JB2RF, where Fig. 10 shows the retrofitted specimen setup. The specimens were heavily instrumented with Linear Variable Differential Transformers (LVDTs) and linear potentiometers to measure displacement at the locations shown in **Figure 8**. Likewise, the strains in the reinforcement and CFRP strains were monitored by using foil-type strain gauges. Full details of the testing programme, instrumentation, retrofitting strategy and experimental results can be found in [36].

Table 1 Material and other characteristics of joint specimens.

ID	f_{cm} (MPa)	f_{ctm} (MPa)	Test condition
JA2	32.0	2.44	Original bare joint, detailing A
JB2	31.3	2.41	Original bare joint, detailing B
JB2RF	55.3	3.67	JB2 retested with new recast core and CFRP retrofit

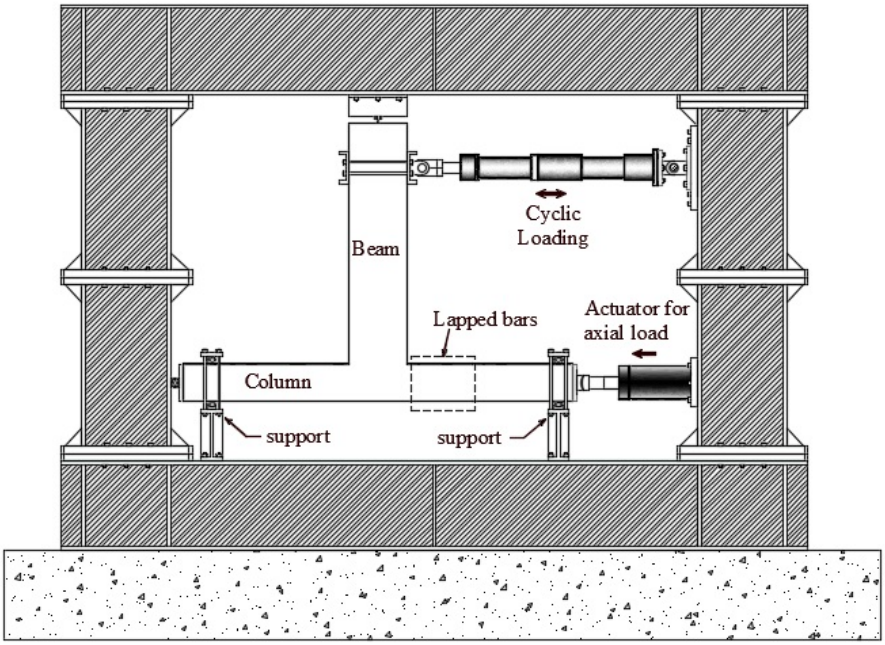

Figure 8: Test setup of bare RC joints (units: mm), adapted from [36].

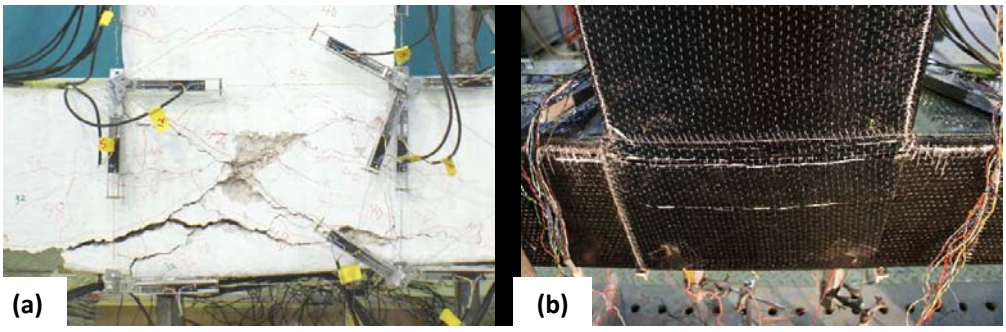

Figure 9: View of final failure mode of (a) bare joints (JB2), and (b) retrofitted joint JB2RF [36].

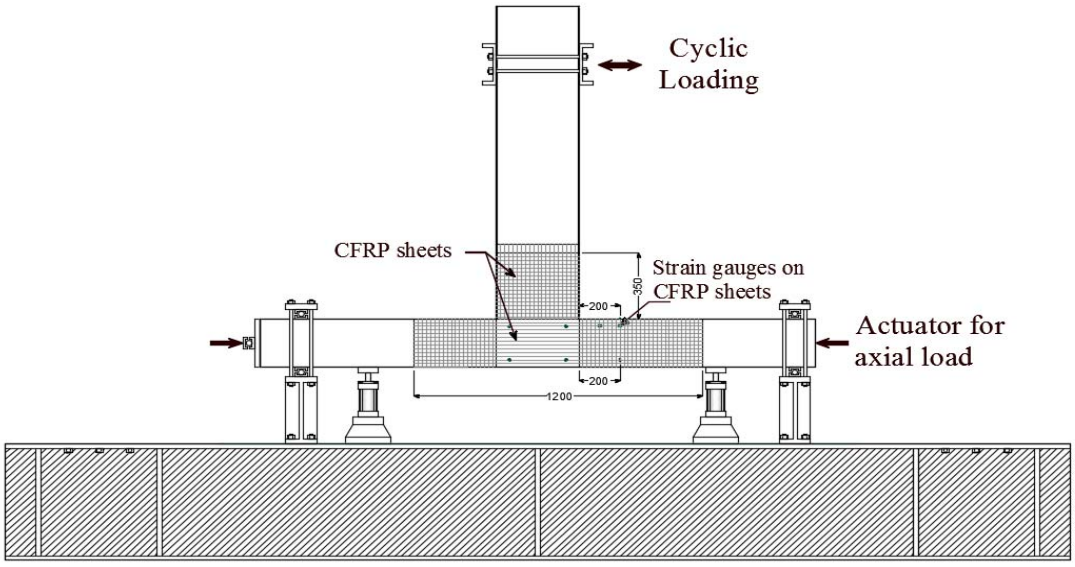

Figure 10: Test setup of retrofitted RC joints (units: mm), adapted from [36].

4. Numerical Model, Results and Discussion

The numerical investigation was performed with the finite element models described in this section. A displacement control algorithm was implemented for all nonlinear analyses with the energy convergence criterion as expressed in Eq. 16. The energy convergence tolerance was set equal to 10^{-5}, which is in line with the numerical implementations presented in [2, 33-35, 39].

$$e_{err} = \frac{\Delta u_s^j \left\| F_s^{t+\Delta t} - R_s^{t+\Delta t} \right\|}{\Delta u_s^1 \left\| F_s^{t+\Delta t} - R_s^t \right\|} \leq tolerance \tag{16}$$

4.1 Finite Element Mesh

Two finite element (FE) meshes were developed for specimens JA2, JB2 and JB2RF so as to investigate the numerical response of the proposed modelling approach. To study the mechanical behaviour of JA2 and JB2, the concrete material was discretized through the use of 8-noded hexahedral isoparametric finite elements, where the steel rebars were discretized with the Natural Beam-Column Flexibility-Based element [34]. A total of 174 concrete and 500 steel beam finite elements were used to discretize the entire bare RC joint. Additionally, 18 hexahedral steel elements (see elements with red colour) were used at the model's boundaries so as to prevent local failure (see Fig. 11). For the retrofitted RC joint (JB2RF), 156 additional hexahedral finite elements were used to mesh the CFRP jacketing that was assumed as fully bonded to the concrete elements (Fig. 12). The FE mesh and material details for the RC joints are given in Tables 2 and 3, respectively.

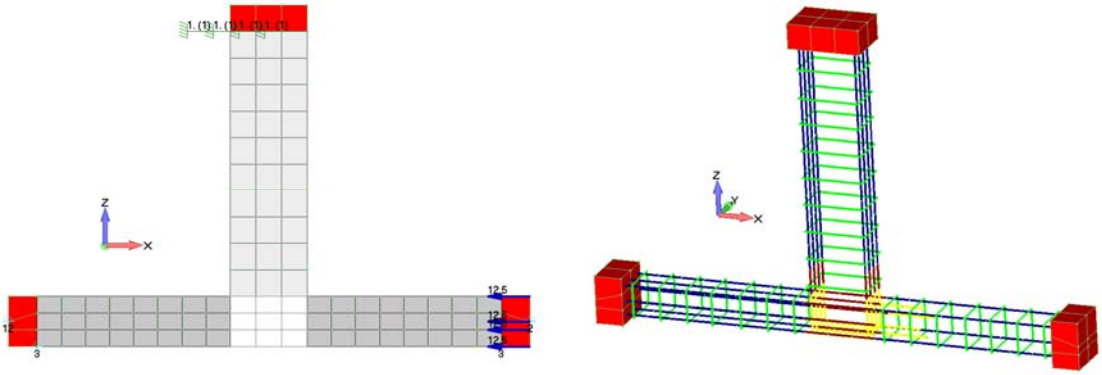

a. b.

Figure 11: Bare RC joints JA2 and JB2. (a) Hexahedral and (b) embedded rebar finite element meshes.

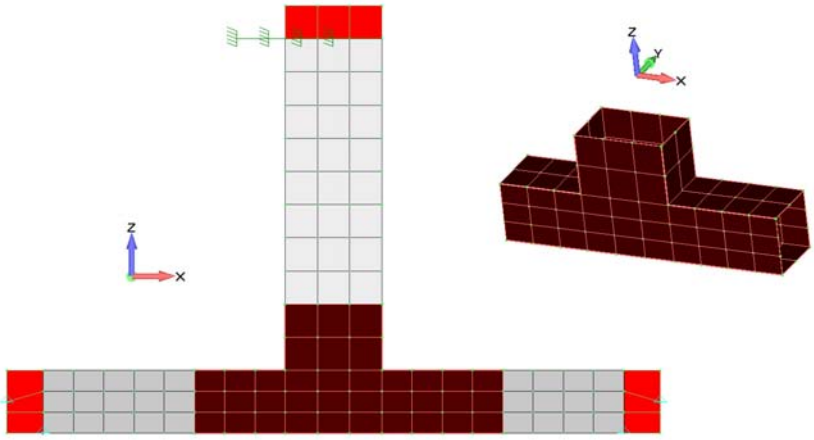

Figure 12: Retrofitted RC joint JB2RF. Concrete and CFRP hexahedral finite element meshes.

It must be noted that specimen JB2 was initially tested until failure, and subsequently rehabilitated with high strength concrete (HSC) and retrofitted with CFRP sheets. The normal strength and HSC domains were discretized and modelled accordingly based on the experiments performed in [36]. Fig. 11 shows the concrete elements used in the modelling: 1) red colour represents the steel hexahedral elements, 2) grey coloured elements correspond to standard concrete, and 3) the white elements represent the HSC domain. All concrete hexahedral elements of JA2 and JB2 (bare RC specimens) were assigned normal concrete material properties, while the concrete hexahedral elements found in the core of JB2RF (shown in white colour) were assigned HSC material properties based on the data provided in Table 3.

Table 2 Finite element mesh details of the RC Joint models.

a/a	Model	Total Number of Nodes	Hexahedral Elements	Embedded Rebar Elements
1	JA2/JB2	396	192	500
2	JB2RF	620	348	500

Table 3 Material details defined within the finite element models.

Material	Young Modulus (GPa)	Hardening Modulus (GPa)	Yielding Stress / Tensile Strength* (MPa)	Compressive Strength (MPa)	Shear remaining strength β	Poisson Ratio	Ultimate Strain ε
Concrete	20	-	2.41*	31.3	0.03	0.2	-
High Strength Concrete	30	-	3.91*	55.3	0.05	0.2	-
Steel Rebars	190	1	551 (Ø16) / 612 (Ø8)	-	-	0.3	15%
CFRP	241	-	4,140*	-	-	0.3	1.7%

4.2 Numerical Results for Bare Joints

According to the experiment [36], the first time-history of imposed cyclic displacements foresaw the application of cycles up to 3% deformation for the case of the JA2 model. This can be seen in Fig. 13, which compares the numerical results and the experimental data, thus shows that the proposed modelling approach reproduces well the test results of the bare RC joint. The extreme pinching observed in the test was also successfully numerically reproduced, indicating that the proposed material damage factors for steel and concrete can capture both material deterioration and bar slippage.

The main differences between the experimental and numerical curves can be attributed to the displacement history that was imposed in a static manner in the cyclic nonlinear analysis, while the experimentally imposed horizontal displacements were not kept constant (due to creep) at each set of cycles, as shown in the experimental curve given in Fig. 13. Therefore, the numerical analysis produced curves with constant horizontal displacements at each set of three cycles. However, the strength deterioration of the numerical model can be clearly observed.

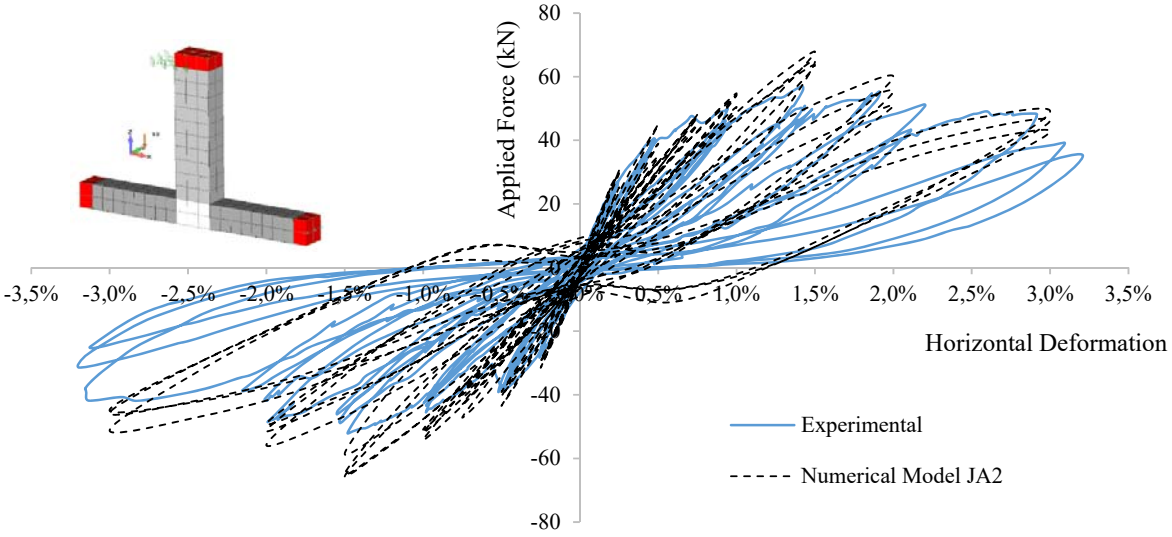

Figure 13: JA2 Joint. Numerical vs experimental P-drift curves.

One of the greatest challenges in computational mechanics is to develop a numerical model that captures the overall mechanical behaviour of RC specimens but at the same time to be able to reproduce experimental measurements at the material level. The most representative physical measure that has its own practical challenges, is the measure of strains at the rebar level. To further compare the numerical and experimental results, the experimentally measured bar strains at two different locations (gauges B19 and B31) within the joint are examined. Fig. 14a shows the gauges that were installed in JA2 on the steel rebars and the corresponding hexahedral elements that were monitored to determine strains (Fig. 14b). It must be noted that the assumption of full bond between the bar and hexahedral concrete finite elements (FEs) implies that the deformation of the two elements is the same. However, the deformation of the steel rebars is expected to be larger than the actual physical deformation according to this numerical assumption, mainly because the damage factors will cause larger deformations on the steel rebar based on the modified material response.

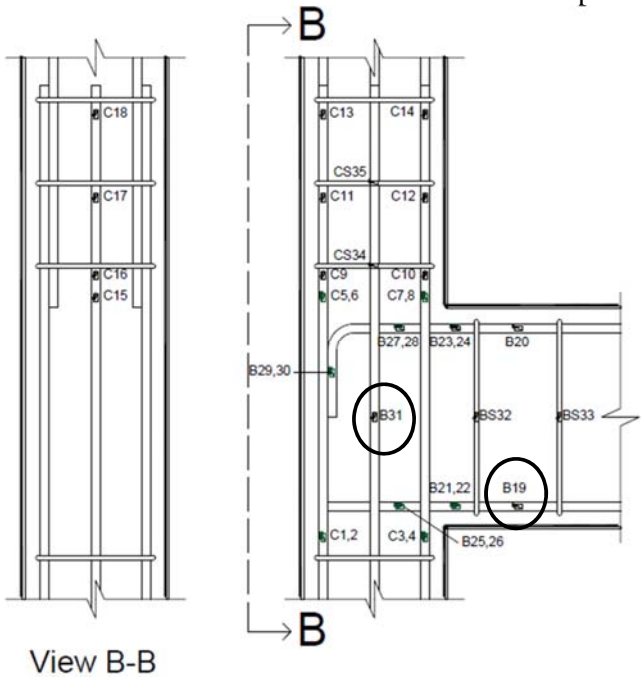

(a)

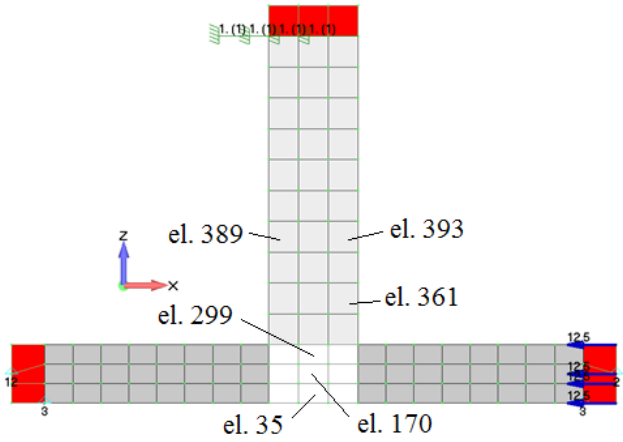

(b)

Figure 14: JA2 Joint. (a) Gauge locations [36] and (b) hexahedral element IDs and locations on the FE mesh.

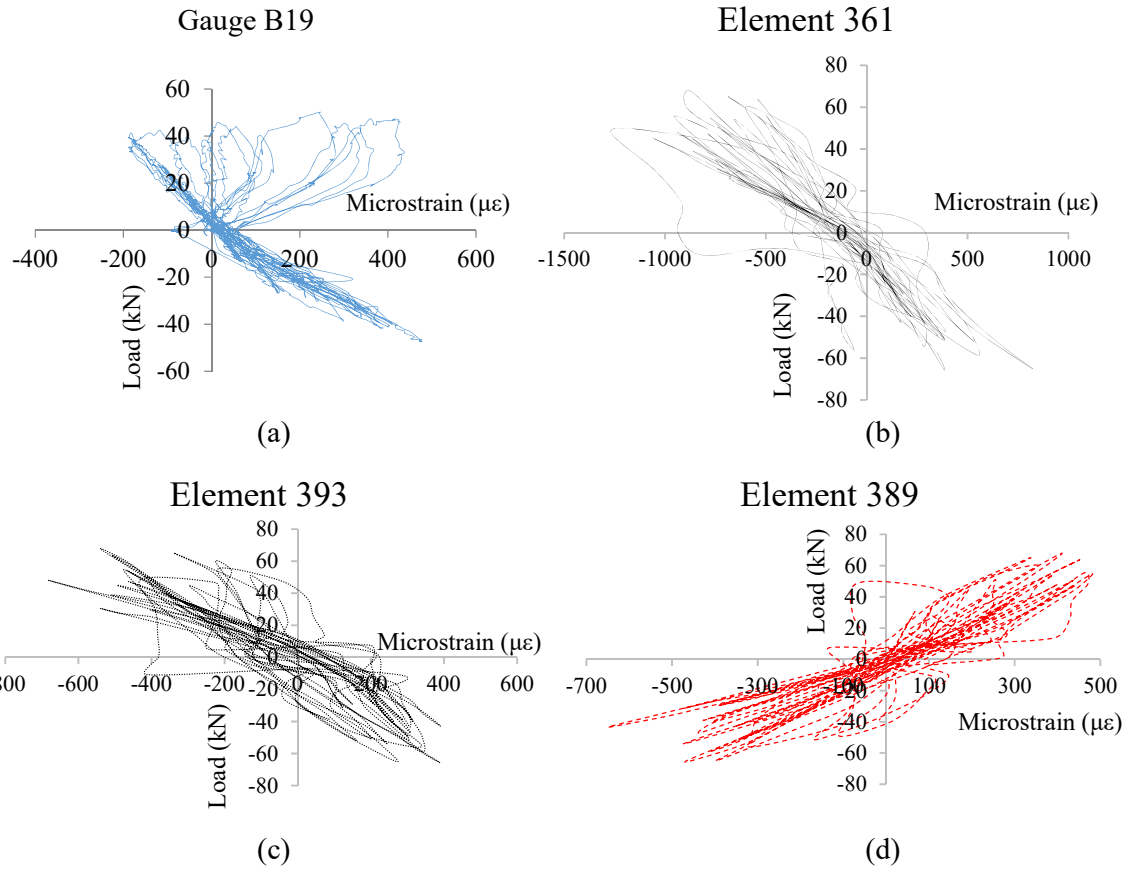

Figure 15: JA2 Joint. ZZ-strain histories of (a) experimental gauge B19, (b) element 361, (c) element 393 and (d) element 389.

Fig. 15 compares the numerically predicted strain history and experimental readings of gauge B19 (see Fig. 15b; ZZ-strain of FE 361). As expected, the predicted strain is higher, which confirms that the damage factors that introduce the material deterioration at the rebar level control this numerical phenomenon.

Figs 15c and 15d show the ZZ-strain of hexahedral elements 393 and 389, respectively. In this case, the numerically computed curves are smaller and closer to the experimental data, given that they are located at areas which are not excessively cracked. Therefore, they represent a mechanical behaviour of an RC volume with insignificant slippage.

Fig. 16 compares the XX-strain computed at hexahedral elements 35, 170 and 299 and the readings

from gauge B31. Even though gauge B31 was located within an area that developed excessive cracking, the bar did not slip excessively. This observation is also reflected in the computed load-strain curves, as shown in Fig. 16. It is important to note that the strains in Fig. 16a highlight the complexity of the problem at hand, where the continuum problem of uncracked concrete is transformed into a concrete domain with significant discontinuities. Nonetheless, the proposed model that incorporates continuum mechanics principles in combination with the smeared crack approach, manages to provide the proposed modelling method with the ability to avoid the use of a discrete modelling method that would have induced significant instabilities and increased computational demand.

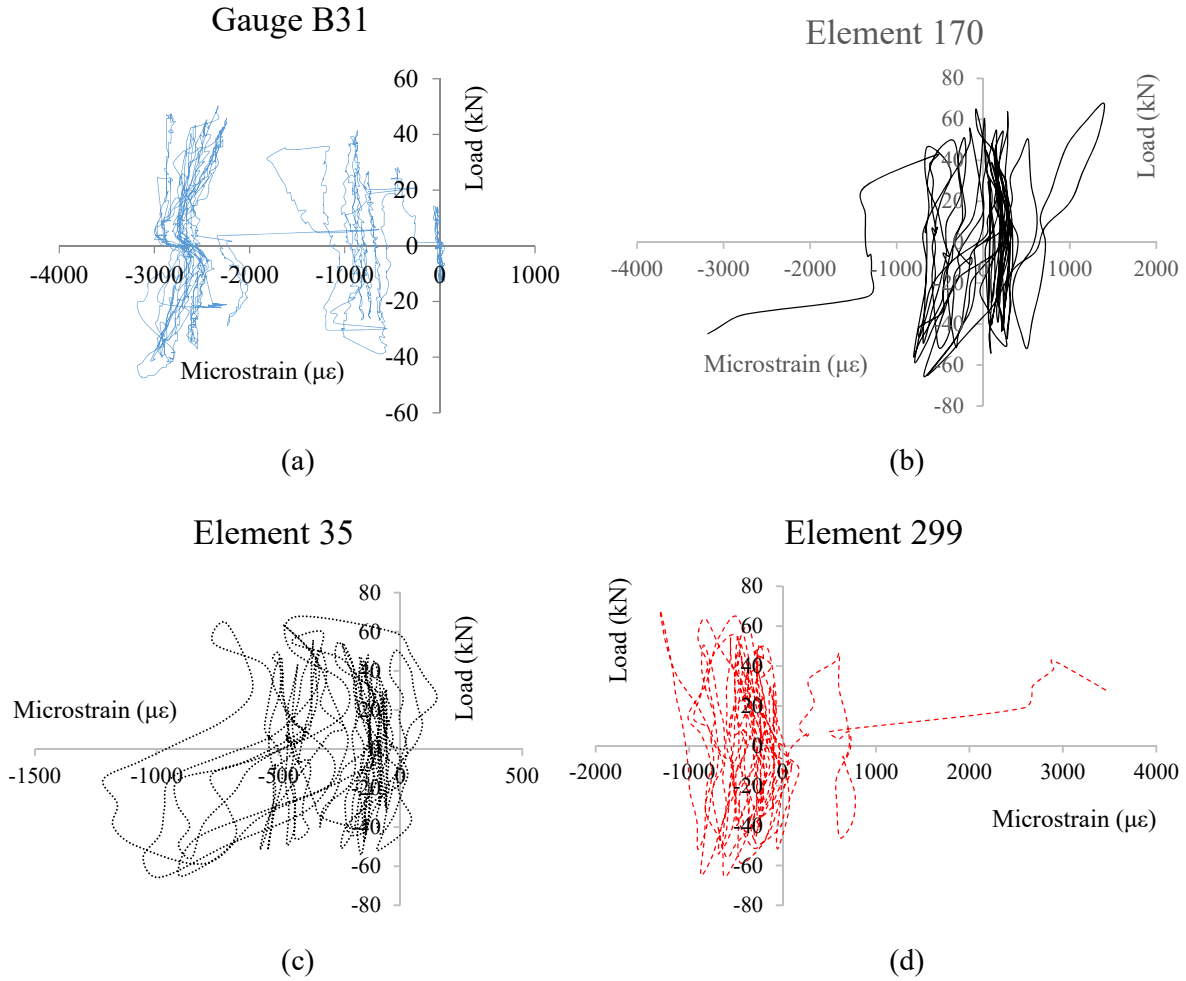

Figure 16: JA2 Joint. XX-strain histories of (a) experimental gauge B31, (b) element 170, (c) element 35 and (d) element 299.

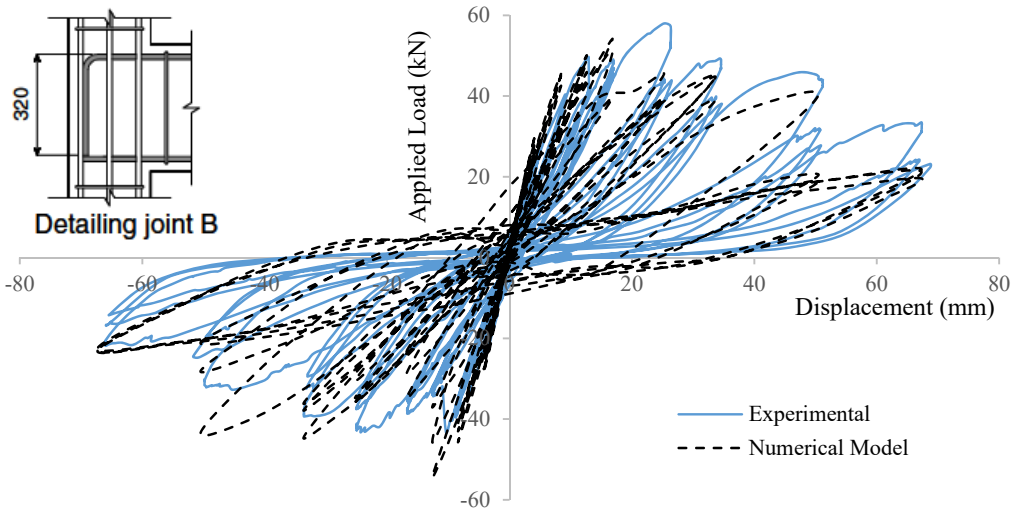

Figure 17: JB2 Joint. Numerical vs experimental P-δ curves.

Fig. 17 compares the experimental and numerical results of joint JB2. It is shown that, in general, the modelling approach captures well the strength deterioration observed in the experiment. The experimental data show a strength drop larger than 50%, also found in the numerical analysis. Especially in the case where the imposed horizontal displacements were larger than 50 mm, the reaction measured along the horizontal direction was found to decrease significantly. According to the experimental data, the maximum computed positive reaction was 58 kN, whilst during the last loading cycle it dropped to 21.8 kN (2.66 times smaller). The corresponding maximum numerically predicted reaction was 54.2 kN, where the respective final reaction during the last loading cycle was computed to be equal to 19.6 kN (2.76 times smaller). Based on these reactions, the numerical model managed to capture the maximum reaction with a 6.6% error, the final reaction during the last cycle with a 10% error, while the overall drop was predicted with a 3.8% error. It is worth mentioning that the extreme nonlinearities, observed in JA2 and JB2, developed during the last loading cycles of the tests were well captured by the proposed modelling method.

4.3 Analysis Results of the Retrofitted Joint

As previously described, after the completion of the JB2 test, the severely damaged substructure was rehabilitated with HSC and retrofitted with CFRP sheets. After retrofitting the damaged specimen, it was renamed into JB2FR and the FE model that was presented in section 4.1 (see Fig. 12) was used to simulate its mechanical response. According to [36], the retrofitted joint was once more subjected to extreme cyclic loading until complete failure. The main goals of the rehabilitation and retrofitting were to double the capacity of the joint, and to achieve a weak-beam strong-column behaviour [36].

Fig. 18 compares the experimental and numerical P-δ curves of JB2FR. The results show that the extreme pinching observed in the experiments were captured well. The maximum experimentally measured positive reaction was 122.5 kN, while the corresponding numerical value was 114.1 kN for a total of 40 mm horizontal imposed displacement. The negative maximum reaction was 125.3 kN, whereas the measured value was 125.8 kN for a negative 40 mm horizontal displacement. This results confirm the ability of the proposed modelling method to reproduce the experimental results of retrofitted substructures that undergo extreme cyclic loading. This also further validates the ability of the proposed algorithm presented in [2, 33, 40] in capturing the mechanical response of CFRP retrofitted RC structures.

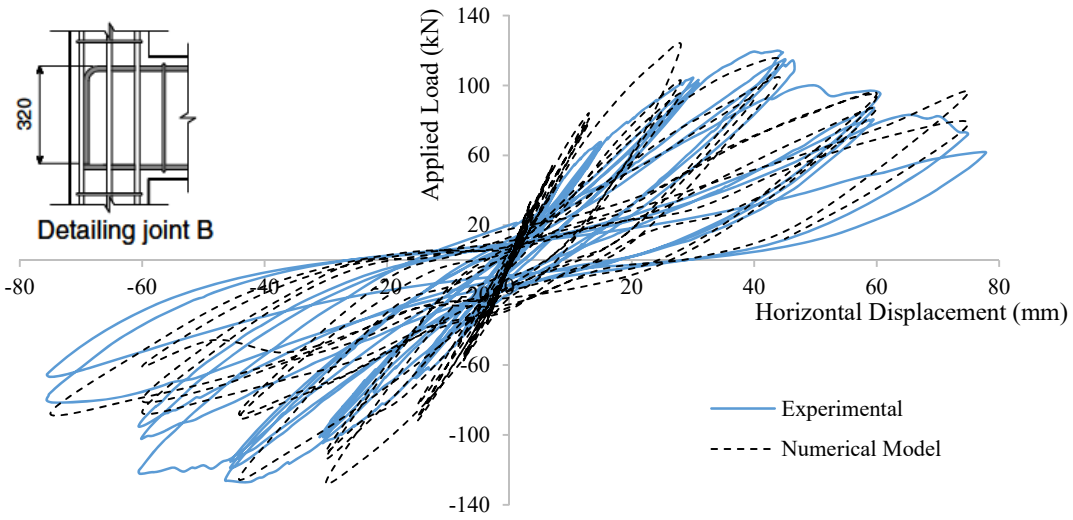

Figure 18: JB2FR Joint. Numerical vs experimental P-δ curves.

Based on the numerically obtained curve in Fig. 18, it is worth mentioning that the numerical model had a stiffer behaviour during the initial cycles (less than 25 mm). This numerical phenomenon can be attributed to the initial concrete damage produced on JB2, which was not accounted for during the numerical analysis of JB2FR. However, this numerical phenomenon was not significant at larger displacements. The challenges of representing the exact geometry and the material properties of a damaged/retrofitted specimen are significant and the level of uncertainty is relatively high. Nonetheless, it is evident that the proposed modelling method can capture the full P-δ curve of the joint at a very acceptable level.

Furthermore, the numerical model managed to capture the drop in-terms of strength with a 9% deviation compared to the experimental curve for the negative horizontal displacement, while the corresponding final positive reactions were computed with a 15% and a 25% error for the last two maximum imposed positive horizontal displacements. This numerical finding is attributed to the initial stiffer behaviour of the numerical model that did not account for the cracked areas of the column and beam members that were developed during the first cyclic test that caused JB2 to fail. Additionally, the full-bond assumption between the CFRP sheets and the concrete surface contributed to this numerical phenomenon as well.

The ability of the proposed model to capture the strains on the CFRP sheets of JB2FR is also studied using the test results. Readings from strain gauges located at the core zone indicated that CFRP strains were close to zero at the initial stages of loading, however, these increased after diagonal cracks developed at the core [36]. Fig. 19 shows that the numerical results match well the experimental readings. According to [36], the CFRP strain at peak load was 7,300 με, while the corresponding numerically predicted value was equal to 6,250 με (see Fig. 20). Finally, the strain for the ultimate horizontal displacement reported in [36] was equal to 16,900 με, where the numerical prediction was 9,600 με. These results indicate that the strain prediction for the peak load was realistic and with an acceptable accuracy of 14%, whereas the ultimate strain at maximum displacement was computed with a variation of 43%. This is attributed to the fact that the numerical model had a stiffer overall behaviour as described above (pre-existing cracks and yielded rebars were not accounted for thus lower strains were developed at the confined concrete volume), whereas the analysis finished half a cycle prior to the application of the last maximum displacement, where the ultimate strain was measured experimentally.

In order to further investigate the strain development at the CFRP sheets, Fig. 21 shows the maximum principal strain and the applied load. The finite element location on the CFRP sheet that was used to develop the graph of Fig. 21, is shown in Fig. 22 and coincides with the location of the gauge used on confining sheets 6 at the midpoint of the lap splice length (see Fig. 10). Based on the load vs strain curves reported in [36] for specimen JC2RF (see Fig. 22), the numerically predicted curves and experimental CFRP strains are found to be in a good agreement. It is important to note that

all three specimens (JA2, JB2) tested in [36] produced a similar behaviour and a respective maximum reaction of approximately 58 to 59 kN. Similarly, JB2RF and JC2RF specimens gave a similar mechanical response in terms of hysteretic behaviour, while both specimens resulted in a maximum reaction of 120 kN, as reported in [36].

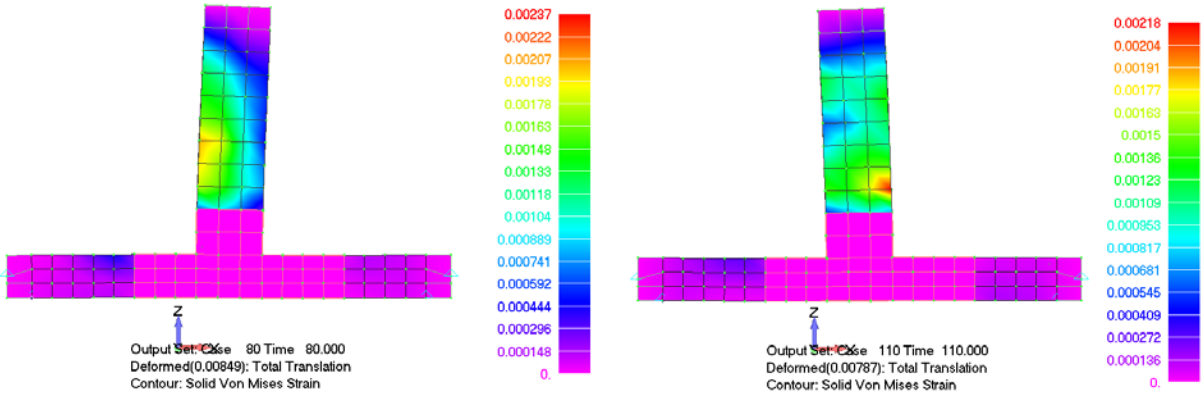

Figure 19: JB2FR Joint. Von Mises strain contour at horizontal displacement (a) 7.5 mm and (b) -7.5 mm.

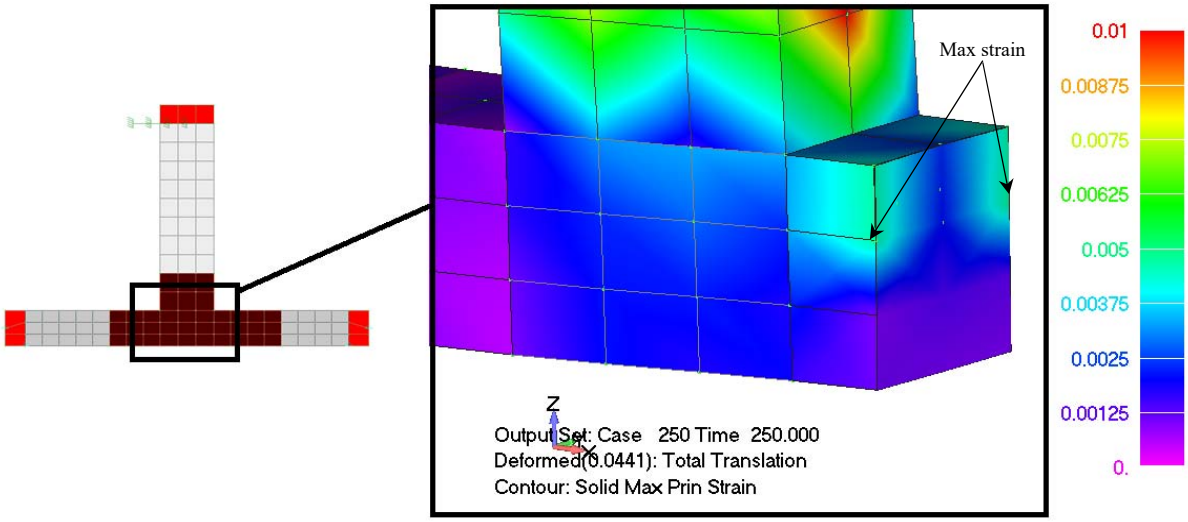

Figure 20: JB2FR Joint. Max principal strain contour at peak load (ε = 6250 με, Pu = 114.13 kN).

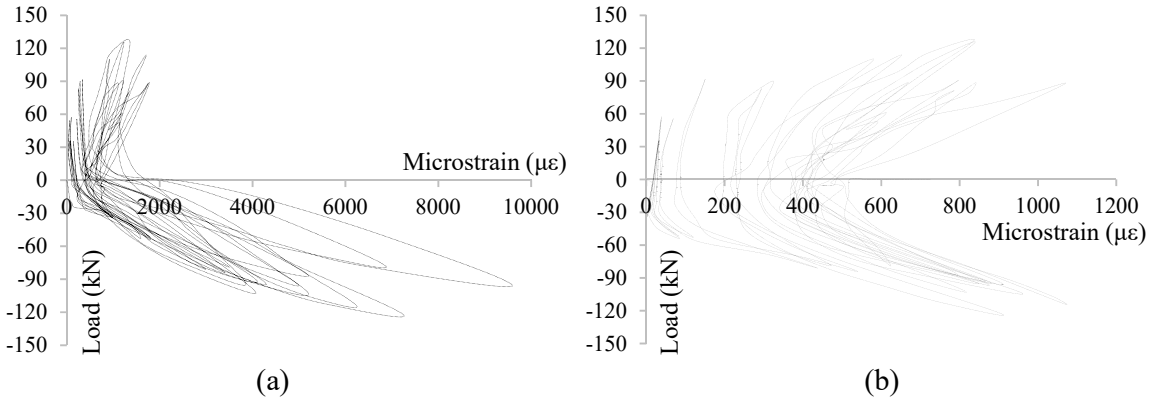

Figure 21: JB2FR Joint. CFRP strain vs load at the (a) core and (b) column lap splices. Numerical results.

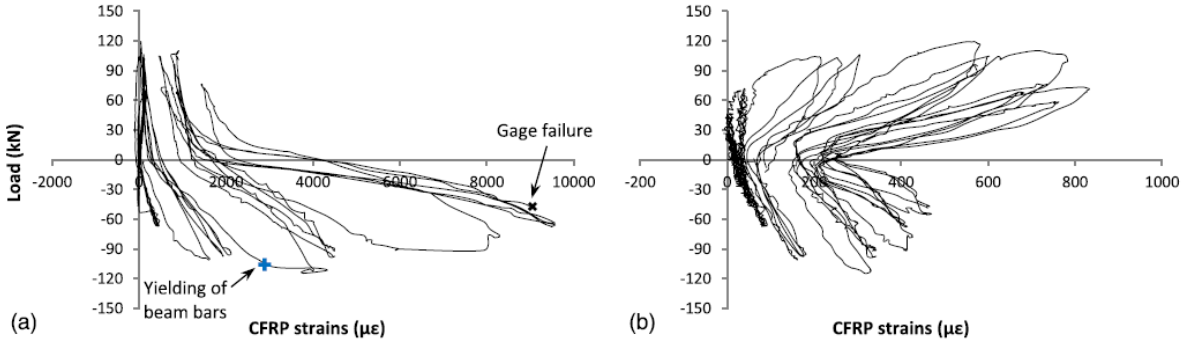

Figure 22: Experimentally recorded strains in CFRP sheets at the (a) core and (b) column lap splices of joint JC2RF [36].

4.4 Computational Efficiency

Table 4 shows the computational demand for different parts of the analysis for the case of the JB2RF model. The total number of internal iterations that were performed during the cyclic nonlinear analysis was 5,513 and for their solution the developed algorithm required 323.9 seconds. This corresponds to a mere 0.059 seconds per internal iteration that characterizes the computational efficiency of the proposed modelling method.

Fig. 23 shows the graph that correlates the obtained internal iterations per displacement increment in an attempt to further illustrate the excessive numerical nonlinearities that this type of problems develop during their cyclic analysis. It is easy to observe that the number of internal iterations are relatively low for horizontally imposed displacements less than 40 mm, where the average internal iteration is equal to 7.7 (per displacement increment). Whereas, when the drift becomes significant for the case of horizontal displacements that are beyond 40 mm, the number of required internal iterations per displacement increment are significantly larger. The average internal iterations per displacement increment in this case is 27.6, which highlights the extreme nonlinearities that occur within the model when the shear deformations are excessive.

Table 4 JB2FR Joint. Required computational times.

a/a	Description	Time (s)
1	Solution of 398 displacement increments (5,513 internal iterations)	323.9
2	Computational Demand per internal iteration	0.059
3	Writing output file	140.7
4	Other	0.7
	Total	465.3

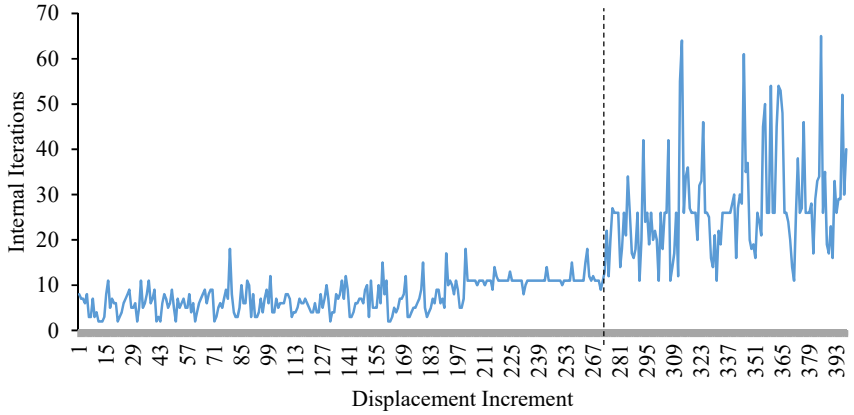

Figure 23: JB2FR Joint. Internal iterations vs displacement increment.

5. Conclusions and Future Work

A new damage factor that accounts for extreme nonlinearities caused by reinforcement bar slippage and excessive concrete cracking is introduced for capturing the mechanical behaviour of bare and retrofitted RC specimens that undergo ultimate limit state cyclic loading. Furthermore, a modification of the concrete material constitutive matrix of crushed hexahedral Gauss Points is proposed for inducing additional numerical stability in excessively cracked concrete regions that are subjected to cyclic loading conditions.

Based on the numerical findings, the proposed modelling method is shown able to capture with an acceptable accuracy the overall mechanical behaviour of both bare and retrofitted RC substructures subjected to extreme cyclic loading. This is achieved without the introduction of additional dofs or bond-slip models that would have complicated and slowed down the numerical procedure. In particular, the ability to capture the pinching effect and strain history or rebars and CFRP sheets is demonstrated through the study of three joint specimens.

A further extension of this work is to study full-scale deficient RC structures under seismic loading. Furthermore, the investigation of the numerical response of the developed model when combined with the HYMOD [2] approach will be performed in the near future.

References

[1] LONDON, Thomson Reuters Foundation, Timeline: World's 14 deadliest earthquakes of last decade, 13th November 13, 2017 https://www.reuters.com/article/us-iran-quake-global/timeline-worlds-14-deadliest-earthquakes-of-last-decade-idUSKBN1DD257

[2] Markou, G. and Papadrakakis, M., (2015), "A Simplified and Efficient Hybrid Finite Element Model (HYMOD) for Non-Linear 3D Simulation of RC Structures", Engineering Computations, 32 (5), pp. 1477-1524.

[3] Markou, G., Mourlas, Ch., Bark, A. and Papadrakakis, M., (2018), "Simplified HYMOD Non-Linear Simulations of a Full-Scale Multistory Retrofitted RC Structure that Undergoes Multiple Cyclic Excitations – An Infill RC Wall Retrofitting Study", Engineering Structures, Vol. 176, pp. 892–916..

[4] Lykidis, G.Ch. and Spiliopoulos K.V. (2008), "3D solid finite element analysis of cyclically loaded RC structures allowing embedded reinforcement slippage", Journal of Structural Engineering-ASCE, 134(4), 629-638.

[5] Tedesco, J. W., Stallings J. M., and El-Mihilmy, M. (1999), "Finite Element Method Analysis of a Concrete Bridge Repaired with Fiber Reinforced Plastic Laminates," Computers and Structures, 72, 379-407.

[6] Arduini M., Di Tommaso A., and Nanni A., "Brittle Failure in FRP Plate and Sheet Bonded Beams," ACI Structural Journal, 94(4), pp. 363-370, 1997.

[7] Kachlakev D., Miller T., Yim S., Chansawat, K. and Tanarat P., Finite Element Modeling of Reinforced Concrete Structures Strengthened with FRP Laminates, Final Report for the Oregon Department of Transportation Research Group and Federal Highway Administration, 2001.

[8] Mostofinejad D. and Talaeitaba S. B. (2006), "Finite Element Modeling of RC Connections Strengthened with FRP Laminates", Iranian Journal of Science & Technology, Transaction B, Engineering, Vol. 30, No. B1, pp. 21-30.

[9] Godat A., Neale K. W. and Labossière P. (2007), "Numerical Modeling of FRP Shear-Strengthened Reinforced Concrete Beams", Journal of Composites for Construction, ASCE, 11(6), pp. 640-649.

[10] Koteš P. and Kotula P. (2007), "Modeling and strengthening of RC bridges by means of CFRP", International Association of Fracture Mechanics for Concrete and Concrete Structures, FraMCos-6 Catania, Italy, 2007 Proceedings, Paper 08-11.

[11] Ibrahim A. M. and Mahmood M. Sh. (2009), "Finite Element Modeling of Reinforced Concrete Beams Strengthened with FRP Laminates", European Journal of Scientific Research,30(4), pp. 526-541.

[12] Chansawat K., Tanarat P., Miller T. H., Yim S. C. and Kachlakev D. I. (2009), "FE Models of GFRP and CFRP Strengthening of Reinforced Concrete Beams", Advances in Civil Engineering, volume 2009, pp. 1-13.

[13] Niroomandi A., Maheri A., Maheri M. R. and Mahini S.S. (2010), "Seismic performance of ordinary RC frames retrofitted at joints by FRP sheets", Engineering Structutres, 32(8), pp. 2326–2336

[14] Young-Min Y.; Ashraf A., M. and Abdeldjelil B. F. (2011), "Three-Dimensional Nonlinear Finite-Element Analysis of Prestressed Concrete Beams Strengthened in Shear with FRP Composites", Journal of Composites for Construction, ASCE, 15(6), pp. 896-907
[15] Sinaei H., Jumaat M. Z. and Shariati M. (2011), "Numerical investigation on exterior reinforced concrete Beam-Column joint strengthened by composite fiber reinforced polymer (CFRP)", International Journal of the Physical Sciences, 6(28), pp. 6572-6579.
[16] Shuraim A. B. (2011), "Efficacy of CFRP configurations for shear of RC beams: experimental and NLFE", Structural Engineering and Mechanics, 39(3), pp. 361-382.
[17] El-Hacha R., Zangeneh P. and Omran H. Y. (2012), "Finite Element Modeling of Steel-Concrete Composite Beams Strengthened with Prestressed CFRP Plate", International Journal of Structural Stability and Dynamics, 12(1), pp. 23-51.
[18] Alhaddad M. S.; Siddiqui N. A.; Abadel A. A.; Alsayed S. H. and Al-Salloum Y. A. (2012), "Numerical Investigations on the Seismic Behavior of FRP and TRM Upgraded RC Exterior Beam-Column Joints", Journal of Composites for Construction, 16(3), pp. 308-321.
[19] Elsanadedy H. M., Al-Salloum Y. A., Alsayed S. H. and Iqbal R. A. (2012), "Experimental and numerical investigation of size effects in FRP-wrapped concrete columns", Construction and Building Materials 29, pp. 56–72.
[20] Elsanadedy H. M., Almusallam T. H., Alsayed S. H. and Al-Salloum Y. A. (2013), "Flexural strengthening of RC beams using textile reinforced mortar – Experimental and numerical study", Composite Structures, 97, pp.40–55.
[21] Milani G. and Lourenço P. B. (2013), "Simple Homogenized Model for the Nonlinear Analysis of FRP-Strengthened Masonry Structures. II: Structural Applications", Journal of Engineering Mechanics, ASCE, 139(1), pp. 77-93.
[22] Anania L. and D'Agata G. (2013), "Numerical investigation on a new CFRP technology for the upgrading of the RC framed structures", Conference: ICCEN2014, Asia-Pacific Chemical, Biological & Environmental Engineering Society.
[23] Dalalbashi A., Eslami A. and Ronagh H. R. (2013), "A numerical investigation on the hysteretic behavior of RC joints retrofitted with different CFRP configurations", Journal of Composites for Construction, 17(3), pp. 271-382.
[24] Gribniak V., Arnautov A. K., Kaklauskas G., Jakstaite R., Tamulenas V. and Gudonis E. (2014), "Deformation Analysis of RC Ties Externally Strengthened with FRP Sheets", Mechanics of Composite Materials, 50(5), pp. 669-676.
[25] Duarte P., Correia J. R., Ferreira J. G., Nunes F. and Arruda M. R. T. (2014), "Experimental and numerical study on the effect of repairing reinforced concrete cracked beams strengthened with carbon fibre reinforced polymer laminates", Canadian Journal of Civil Engineering, 41, pp. 222–231.
[26] Nasr Z. H., Alaa G. S., Amal H. Z. (2015), "Finite element analysis of reinforced concrete beams with opening strengthened using FRP", Ain Shams Engineering Journal, https://doi.org/10.1016/j.asej.2015.10.011
[27] Qapo M., Dirar S., Yang J. and Elshafie M. Z. E. B. (2015), "Nonlinear finite element modelling and parametric study of CFRP shear-strengthened prestressed concrete girders", Construction and Building Materials, 76, pp. 245–255.
[28] Mrozek M., Mrozek D. and Wawrzynek A. (2015), "Numerical analysis of selection of the most effective configuration of CFRP composites reinforcement of masonry specimens", Composites Part B: Engineering, 70, pp. 189–200.
[29] Mazzucco G., Salomoni V. A., Majorana C. E., Pellegrino C. and Ceccato C. (2016), "Numerical investigation of concrete columns with external FRP jackets subjected to axial loads", Construction and Building Materials, 111, pp. 590–599.
[30] Azarm R., Maheri M. R. and Torabi A. (2016), "Retrofitting RC Joints Using Flange-Bonded FRP Sheets", Iranian Journal of Science and Technology, Transactions of Civil Engineering, 41(1), pp 27–35.
[31] Banjara N. K. and Ramanjaneyulu K. (2017), "Experimental and numerical investigations on the performance evaluation of shear deficient and GFRP strengthened reinforced concrete beams", Construction and Building Materials, 137, pp. 520–534.
[32] Cortés-Puentes W. L. and Palermo D. (2012), "Modeling of RC Shear Walls Retrofitted with Steel Plates or FRP Sheets", Journal of Structural Engineering, ASCE, 138(5), pp. 602-612.
[33] Mourlas, C., Markou, G. and Papadrakakis, M. (2019), "Accurate and Computationally Efficient Nonlinear Static and Dynamic Analysis of Reinforced Concrete Structures Considering Damage Factors", Engineering Structures, 178 (2019), pp. 258–285.

[34] Markou G., Papadrakakis M. (2013), "Computationally efficient 3D finite element modeling of RC structures", Computers and Concrete, 12(4), 443–98.
[35] Mourlas, Ch., Papadrakakis M. and Markou, G. (2017), "A Computationally Efficient Model for the Cyclic Behavior of Reinforced Concrete Structural Members", Engineering Structures, 141, pp. 97–125.
[36] Garcia, R., Jemaa, Y., Helal; Y., Guadagnini, M. and Pilakoutas, K. (2014), "Seismic Strengthening of Severely Damaged Beam-Column RC Joints Using CFRP", Journal of Composites for Construction, 18(2), 04013048.
[37] Willam K. J. and Warnke E. P., (1974), "Constitutive model for the triaxial behaviour of concrete", Seminar on concrete structures subjected to triaxial stresses, Instituto Sperimentale Modeli e Strutture, Bergamo, Paper III-1.
[38] Menegotto, M., and Pinto, P. E. (1973). "Method of analysis for cyclically loaded reinforced concrete plane frames including changes in geometry and non-elastic behavior of elements under combined normal force and bending." Proceedings, IABSE Symposium on Resistance and Ultimate Deformability of Structures Acted on by Well Defined Repeated Loads, Lisbon, Portugal, 15–22.
[39] Markou, G., AlHamaydeh, M. (2018), 3D Finite Element Modeling of GFRP-Reinforced Concrete Deep Beams without Shear Reinforcement, International Journal of Computational Methods, 15(1), pp. 1-35.
[40] Markou, G., Mourlas, C. and Papadrakakis, M. (2017), "Cyclic Nonlinear Analysis of Large-Scale Finite Element Meshes Through the Use of Hybrid Modeling (HYMOD)", International Journal of Mechanics, 11(2017), pp. 218-225.